Letters

A Practical Approach to Mitigate Low-Frequency Oscillation in Railway Electrification Systems

Haitao Hu, *Member, IEEE*, Yi Zhou, *Student Member, IEEE*, Jie Yang, Zhengyou He, *Senior Member, IEEE*, and Shibin Gao

***Abstract*—The low-frequency oscillation (LFO) phenomenon has frequently happened in the railway electrification systems (RES), which often caused the traction atresia of electric trains and protection malfunction of traction network. In this letter, a practical mitigation approach is presented based on impedance analysis, which indicates that changing the operation mode of the electric trains to diode-bridge rectification (DBR) circuit can mitigate the LFO because the impedance of the rectifier is increased. Then, combining the Prony technology, an online identification and mitigation approach, is proposed here for mitigating the LFO phenomenon. Experimental results verify the effectiveness of the proposed method in stabilizing voltage fluctuation of the RES. This method can also identify the oscillatory frequency and the corresponding attenuation factor.**

***Index Terms*—Diode-bridge rectification (DBR), low-frequency oscillation, railway electrification systems (RES).**

I. Introduction

THE low-frequency oscillation (LFO) has frequently occurred in the railway electrification systems (RES) when multiple electric trains simultaneously energized in a rail depot [1]. The LFO in the RES easily occurs under the condition of the weak supply network and multiple electric trains. At this time, only the four-quadrant converters (4QCs) of electric trains and their auxiliary systems were operating. In addition, according to the measured data, the electric trains worked in a light-power condition. This is an important feature of the LFO in the RES. The LFO phenomenon has caused a number of serious consequences, such as the malfunction of the protection system, high voltage and current that damage onboard devices, and delay

Manuscript received October 8, 2017; revised November 11, 2017 and January 7, 2018; accepted January 30, 2018. Date of publication February 7, 2018; date of current version July 15, 2018. This work was supported in part by the National Key Research and Development Program of China under Grant 2017YFB 1200802, and in part by the National Natural Science Foundation of China under Grant NSFC 51677154 and Grant 51525702. *(Corresponding author: Zhengyou He.)*

The authors are with the School of Electrical Engineering, Southwest Jiaotong University, Chengdu 610031, China (e-mail: hht@swjtu.edu.cn; zhouyipower@163.com; jdyj@my.swjtu.edu.cn; hezy@swjtu.edu.cn; gao_shi_bin@126.com). (e-mail:

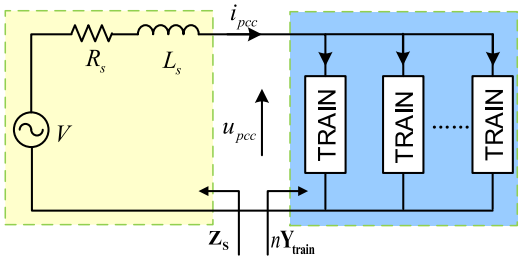

Fig. 1. Train-network system equivalent model.

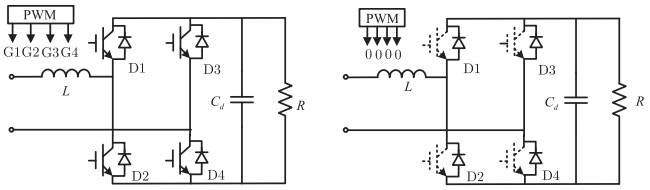

Fig. 2. Circuit structure of the two modes. (a) Normal mode. (b) DBR mode.

tion network is expressed as

$$T = \frac{nZ_s}{Z_{\text{train}}} = nZ_s \cdot Y_{\text{train}} \tag{1}$$

where n is the number of electric trains energized in a rail depot.

The interactions between the electric train and the traction network can be analyzed by plotting the frequency responses of the Z_s and Z_{train} [4]. The traction network and the electric trains are stable when they operate separately. The system stability will be dependent on the phase difference at the frequencies where their magnitude responses intersect. The phase margin (PM) at the intersection point f_i could be defined as

$$\text{PM}\,(f_i) = 180^\circ - [\angle Z_s\,(f_i) - \angle Z_{\text{train}}\,(f_i)]. \tag{2}$$

The impedance of the load module is reduced when multiple electric trains energize in parallel. It is possible to make PM ≤ 0 at the intersection point f_i and cause the train-network system unstable. If the impedance of the source module is always smaller than that of the load module, the system is always stable due to nonexistent intersection point. Therefore, it is effective to reduce the observed impedance of the traction network and increase the equivalent impedance of electric trains for suppressing the LFO. In fact, the cost of reducing the impedance of the traction network is exorbitant. In addition, it is infeasible to change the impedance of the electric train through regulating the control parameters in real time. Consequently, this letter proposes utilizing the DBR mode to change the impedance of the 4QC in real time. Fig. 2 shows that the DBR mode is similar to the normal mode in the circuit structure. When the output control signals of the digital controller are low level, the IGBTs will turn OFF and the antiparallel diodes can constitute the DBR circuit. The equivalent impedance of the electric train is shown in Fig. 3 under different modes.

The equivalent impedance of the electric train in the DBR mode is larger than that in normal mode and no intersection

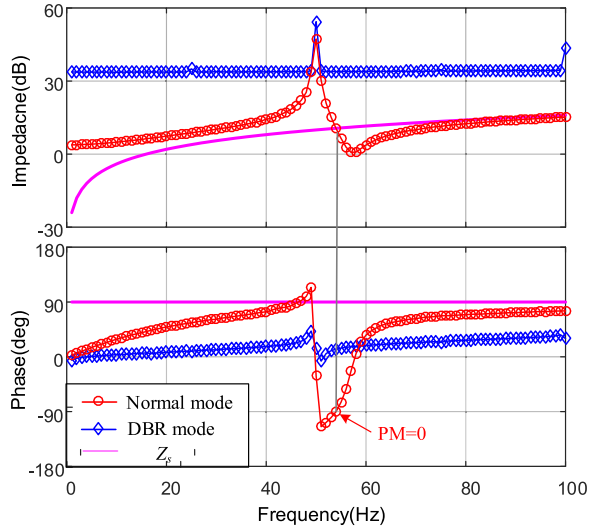

Fig. 3. Equivalent impedance of the 4QC in different modes by frequency scan.

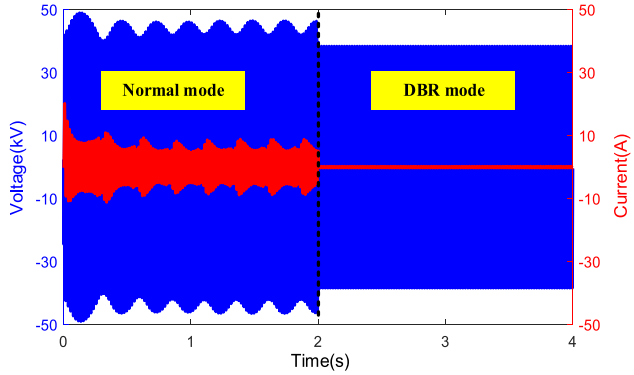

Fig. 4. Time-domain simulation result in different modes.

point with the traction network. Theoretically, this method can suppress the LFO because the impedance of the electric train is increased. The time-domain simulation result is shown as Fig. 4. In the normal mode, the amplitude of the traction network side (TNS) voltage and current appear as violent oscillation. When the 4QC becomes the DBR mode, the oscillation disappears and the TNS current is small due to the light-power working condition. The dc-link voltage drops when the mode of 4QC becomes the DBR mode, but the dc-link capacitance can keep the dc voltage skill smooth due to the filtering scheme. Additionally, it should be noted that the DBR mode cannot bring additionally serious harmonic problems. The first reason is that the injecting current of the electric train is comparably small in light-power conditions. In addition, when one electric train works in the DBR mode, it mainly causes the third, fifth, seventh, and ninth harmonic currents injecting into the traction network. These harmonic currents are the same with the background harmonics of the utility power system. In the actual traction network, the power filters can suppress them well. Consequently, this method can suppress the LFO effectively without causing additional harmonic problems in the light-power condition.

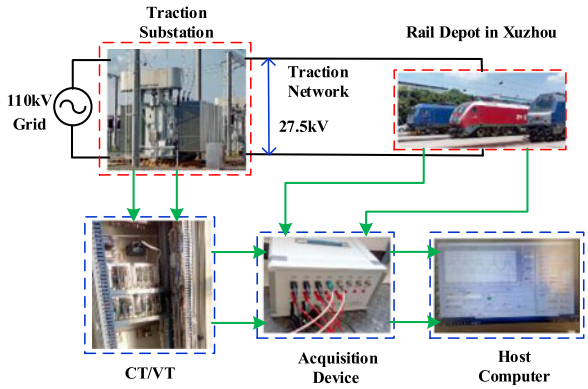

Fig. 5. Actual test setup in Xuzhou rail depot.

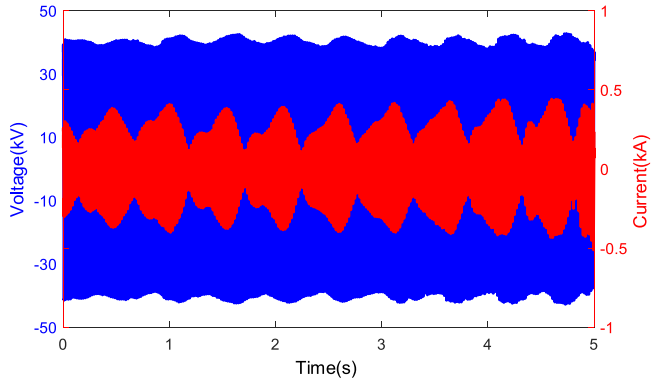

Fig. 6. Measured waveform of the LFO in Xuzhou.

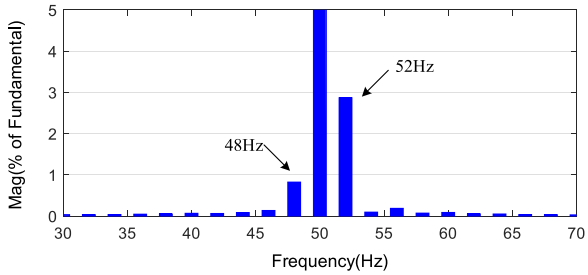

Fig. 7. FFT result of the measured voltage data in Xuzhou.

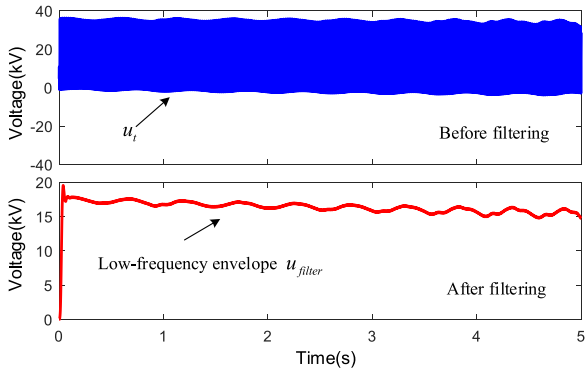

Fig. 8. Transformed result and the LFO envelope.

B. Detection Method of the LFO

Under the operation mode, a detection method that can accurately identify the LFO is presented to provide a trigger signal for the suppression method. In reference to the identification method of the LFO in power systems, the Prony algorithm is selected. This algorithm uses the linear combination of p exponential functions with the arbitrary amplitude, phase, frequency, and attenuation factor to fit the sample signals $x(n)$

$$\hat{x}(n) = \sum_{i}^{p} b_i z_i^n \quad (n = 0, 1 \ldots N-1)$$

$$\begin{cases} b_i = A_i \exp(j\theta_i) \\ z_i = \exp\left[(d_i + j2\pi f_i)\,\Delta t\right] \end{cases} \tag{3}$$

where p is the model order, Δt is sampling interval, A_i, θ_i, d_i, and f_i are the amplitude, phase, attenuation factor and frequency, respectively. Here, $\hat{x}(n)$ is approximated value of $x(n)$. A_i, θ_i, d_i, and f_i can be obtained using the detailed solution steps in [5], [6].

The TNS voltage waveform shows a low-frequency envelope of f_1. It is another important feature of the LFO in the RES. Practically, the TNS voltage waveform contains massive $f_0 \pm f_1$ interharmonic components instead of the low-frequency f_1 component [1]. Two symmetrical oscillation modes $(f_0 \pm f_1)$ can be obtained using the TNS sample signals. It is unconducive to judge the real oscillatory situation because attenuation factors of two modes may be different. In addition, rich high-frequency components in the TNS sample signals reduce the signal-to-noise ratio of the signals and make the Prony analysis unstable. Therefore, some pretreatment steps are needed to keep the algorithm stable.

1) The first step of the pretreatment steps is using a low-pass filter to remove high-frequency components.
2) The second step of the pretreatment steps is transforming original sample signals. Specific transformation processes are shown in Appendix A.

In order to verify the effectiveness of the algorithm, the data measured in the Xuzhou traction substation are utilized to test the algorithm. The actual test setup is shown in Fig. 5. The acquisition device is connected to the monitor cabinet in the traction substation. The voltage and the current data can be shown on the display interface and recorded in real time. The measured waveform of the LFO is shown as Fig. 6. The FFT result in Fig. 7 shows that the TNS voltage waveform contains massive 48 and 52 Hz interharmonic components. Therefore, the low-frequency envelope is about 2 Hz. Fig. 8 shows the transformation results of the TNS voltage by using pretreatment steps. After filtering, the low-frequency envelope is extracted effectively. Moreover, the identification results are listed in Table I. It shows that the

TABLE I
IDENTIFICATION RESULTS

Oscillatory frequency (Hz)	Attenuation factor	Order of model
2.0127	0.2137	41

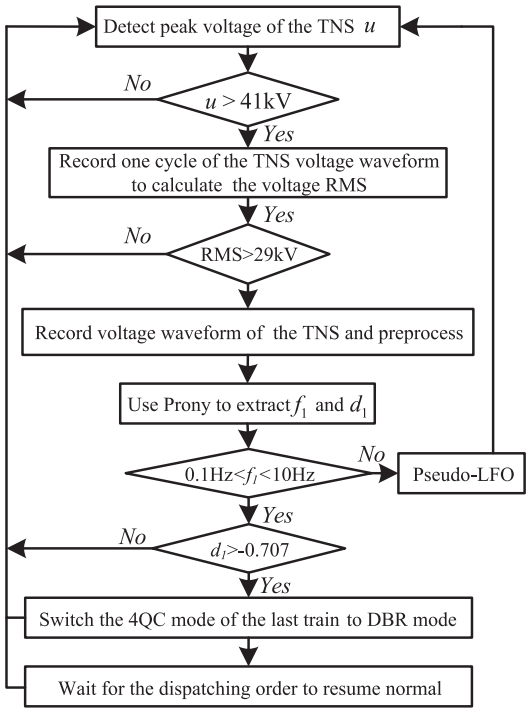

Fig. 9. Flow chart of the mitigation approach.

identification method can get the oscillatory frequency and attenuation factor accurately.

C. Mitigation Procedure

In summary, the mitigation approach dealing with the LFO in the RES is then presented and arranged in Fig. 9.

The LFO frequency is normally 0.1–10 Hz in the RES [1]. A 2-s recording voltage waveform is enough to identify almost all LFO frequencies. In addition, according to the code for design of railway traction power supply in China, the safe operation time cannot exceed 5 min under the TNS voltage that is more than 29 kV (peak voltage is $29 \times \sqrt{2} \approx 41$ kV). The threshold of the TNS peak voltage is set to 41 kV. The root mean square (r.m.s.) is calculated to avoid the maloperation of the protection system due to instantaneous voltage spike. Theoretically, if the attenuation factor is less than zero, the oscillatory amplitude will attenuate. However, considering the numerical error of the calculation and the accelerate decay, a conservative attenuation factor -0.707 is selected as the threshold. The duration of the voltage oscillation is shorter if attenuation factor is less than -0.707. When the TNS voltage becomes oscillation, the 4QC of the latest energized electric train is automatically switched in the DBR mode. It will resume normal rectification mode if the oscillatory voltage recovered and one or more electric trains run away.

D. Technologies Comparison

The suppression technologies for mitigating LFO in the RES can be divided into three categories, i.e., grid enhancement, control parameters optimization, and additional device placement. The grid enhancement is to reduce the impedance of the traction network such as increasing the capacity of the main transformer in the traction substation. The control parameters optimization is to change the impedance of the electric trains. The additional device placement is to make dynamic adjustment of the system such as the power oscillation damper controller. The proposed method changes the operation modes to increase the impedance of the electric trains and make the rectifiers passive in real time. In terms of cost, mitigation performance, and real-time performance, the comparisons of these solutions are summarized in Table II.

TABLE II
TECHNOLOGIES COMPARISONS DEALING WITH THE LFO

Method	Cost	Performance	Real time
Grid enhancement	High	Good	No
Additional device placement	Moderate	Insufficient	Yes
Control parameters optimization	Low	Moderate	No
Operation mode adjustment	Low	Good	Yes

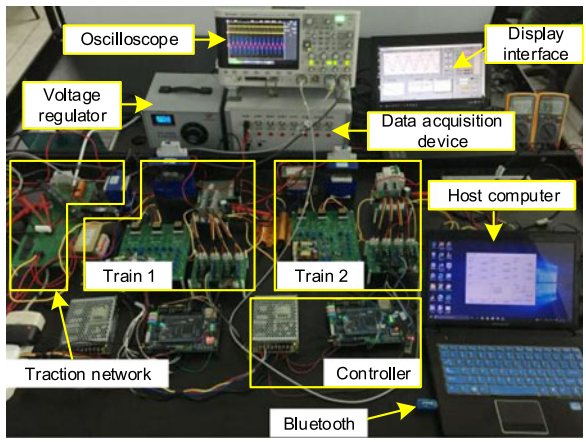

Fig. 10. Equivalent experimental system.

The proposed method is low cost without adding other devices and shows good mitigation performance. Moreover, it is able to detect and suppress the LFO in real time.

III. EXPERIMENTAL VERIFICATION

An experimental system consisting of the equivalent traction network and rectifiers has been employed to evaluate the effectiveness of the mitigation approach. The experimental system is shown in Fig. 10. The detailed electrical parameters are listed in Table III.

When the LFO is induced, the data acquisition device will record the TNS voltage data and calculate the attenuation factor and the oscillatory frequency. If they satisfy the decision condition, a signal will be sent to the host computer by Bluetooth and the control pulse signal will be blocked. The voltage and current waveforms of the experimental system is shown as Fig. 11.

In the normal the mode, the TNS peak voltage and the peak current are about 310 V and 0.4 A, respectively. When the oscillation occurs, they reach about 390 V and 1 A, respectively. Obviously, the TNS peak voltage exceeds the threshold and the

TABLE III
PARAMETERS OF THE EXPERIMENTAL

Symbol	Description	Value
u	TNS voltage	220 V
f_0	Fundamental frequency	50 Hz
L	Inductance of rectifier	0.014 H
R	Load of rectifier	50 Ω
R_s	Equivalent resistance of traction network	1.5 Ω
L_s	Equivalent inductance of traction network	0.23 H
C_s	Equivalent Capacitance of traction network	0.15 μF
C_d	dc-link Capacitance	0.009 F
u_{dc}	dc voltage	40 V
Kp_{vc} Ki_{vc}	Control parameters of voltage loop	$Kp_{vc} = 0.1$ $Ki_{vc} = 0.002$
Kp_{cc} Ki_{cc}	Control parameters of current loop	$Kp_{cc} = 4.5$ $Ki_{cc} = 0.15$
f_s	Sampling frequency	20 kHz
u_{th}	The peak voltage threshold	330 V
u_{rms}	The r.m.s. voltage threshold	233 V

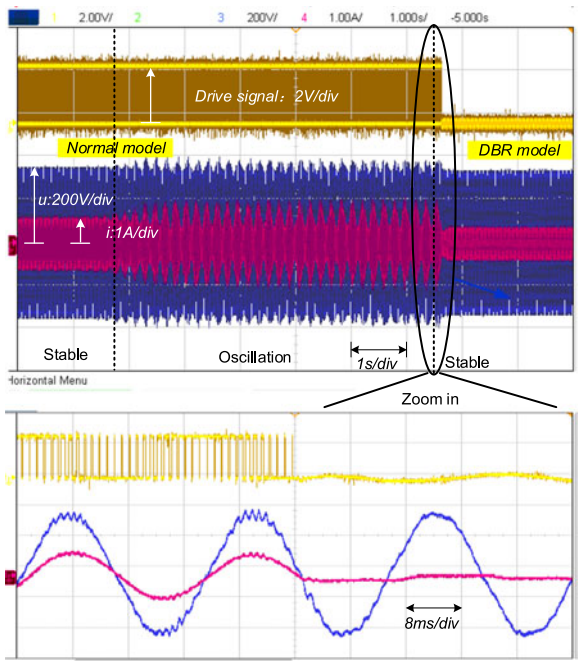

Fig. 11. TNS voltage waveform of experimental system.

identification program is triggered. After control pulses blocked, the oscillation is suppressed effectively and an obvious reduction of the TNS current can be found in Fig. 11. The reason is that the reduction of the dc voltage will cause the power drop when the dc-side load is a pure resistance.

Fig. 12 shows the low-frequency envelope extracted with pretreatment steps and the detection time. When the data acquisition device is triggered recording, the timing signal is high level. When the pulses are blocked, the timing signal becomes low level. Consequently, the time of one complete operation including acquisition and calculation is recorded. The FFT

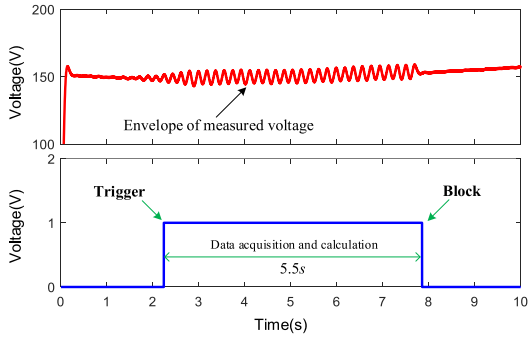

Fig. 12. Low-frequency envelope of the TNS voltage and operation time of the detector.

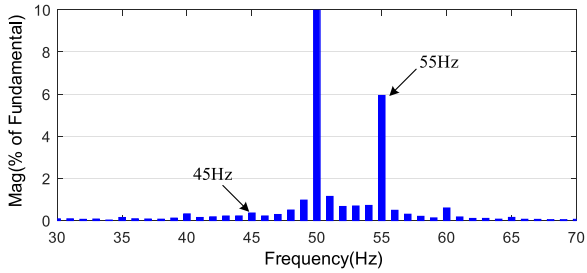

Fig. 13. FFT result of the experimental TNS voltage.

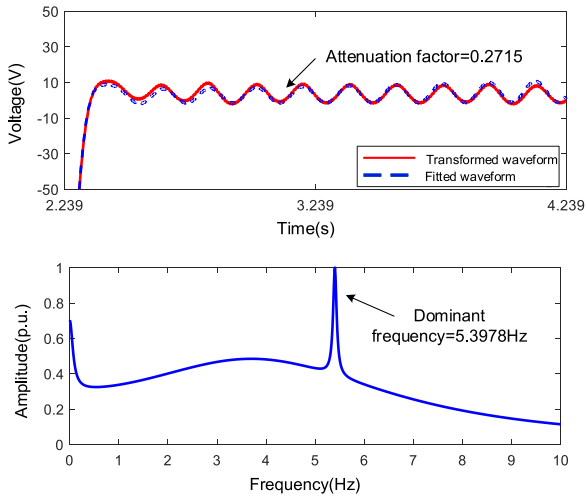

Fig. 14. Fitted result and oscillatory frequency.

result of the experimental TNS voltage shows that the oscillatory frequency is about 5 Hz in Fig. 13.

The dominant mode of the LFO in the RES is considered at the maximum amplitude-frequency response at 0–10 Hz. Thus, the dominant frequency is the oscillatory frequency. In Fig. 14, according to the fitted result of the 2-s record data, the oscillatory frequency and the attenuation factor can be obtained by the Prony algorithm.

IV. CONCLUSION

A practical LFO mitigation approach is presented here. The proposed approach can change the impedance of the

electric trains in real-time to effectively and practically suppress the LFO. Experimental results verify that the approach can effectively suppress voltage fluctuation in the traction network and identifies oscillation frequency and attenuation factor, while it avoids the traction atresia and protection malfunction.

APPENDIX

Supposing the TNS voltage is expressed as follows:

$$u = U_0 \cos(2\pi f_0 t) + U_1 \cos[2\pi (f_0 + f_1) t] + U_2 \cos[2\pi (f_0 - f_1) t]. \quad (4)$$

A cosine signal is then generated using the local clock of controller as follows:

$$u_{\mathrm{clk}} = \cos(2\pi f_0 + \varphi). \quad (5)$$

In (4) and (5), f_0, U_0 are the fundamental frequency, phase and amplitude of the TNS, respectively. U_1 and U_2 are the amplitudes of the oscillatory voltage. φ is the initial phase difference of the TNS fundamental voltage and the cosine signal.

Combining (4) and (5) yields

$$\begin{aligned} u \times u_{\mathrm{clk}} = {} & \frac{1}{2}U_0 [\cos(4\pi f_0 t + \varphi) + \cos(\varphi)] \\ & + \frac{1}{2}U_1 \{\cos[(4\pi f_0 + 2\pi f_1) t + \varphi) + \cos(2\pi f_1 t - \varphi)]\} \\ & + \frac{1}{2}U_2 \{\cos[(4\pi f_0 - 2\pi f_1) t + \varphi) + \cos(2\pi f_1 t + \varphi)]\}. \end{aligned} \quad (6)$$

100 Hz is the primary component in (6) and the transformed voltage u_t is obtained by adopting a low-pass filter.

$$u_t = \frac{1}{2}U_0 \cos(\varphi) + \frac{1}{2}U_1 \cos(2\pi f_1 t - \varphi) + \frac{1}{2}U_2 \cos(2\pi f_1 t + \varphi). \quad (7)$$

The filtered waveform only contains dc component and low-frequency f_1 component. As (7) includes the initial phase difference, the amplitude information will be lost after transforming. But the other information can be retained. Consequently, the oscillatory frequency and attenuation factor are then identified clearly by using the Prony algorithm. The transformed approach provides an accurate reference signal for LFO determination.

ACKNOWLEDGMENT

The authors would like to thank C. P. Zhao of the Shanghai Railway Bureau for his assistance with the measurement work.

REFERENCES

[1] H. Hu, H. Tao, F. Blaabjerg, X. Wang, Z. He, and S. Gao, "Train-Network Interactions and Stability Evaluation in High-Speed Railways–Part I: Phenomena and Modeling," *IEEE Trans. Power Electron.*, vol. 33, no. 6, pp. 4627–4642, Jun. 2018.

[2] R. D. Middlebrook, "Input filter considerations in design and application of switching regulators," in *Proc. IEEE Ind. Appl. Soc. Conf.*, Oct. 1976, pp. 94–107.

[3] C. M. Wildrick *et al.*, "A method of defining the load impedance specification for a stable distributed power system," *IEEE Trans. Power Electron.*, vol. 10, no. 3, pp. 280–285, May 1995.

[4] X. Wang, L. Harnefors, and F. Blaabjerg, "A unified impedance model of grid-connected voltage-source converters," *IEEE Trans. Power Electron.*, vol. 33, no. 2, pp. 1775–1787, Feb. 2018.

[5] S. Zhao and K. A. Loparo, "Forward and backward extended prony (FBEP) method for power system small-signal stability analysis," *IEEE Trans. Power Syst.*, vol. 32, no. 5, pp. 3618–3626, Sep. 2017.

[6] S. Rai *et al.*, "Estimation of low-frequency modes in power system using robust modified Prony," *IET Gener. Transmiss. Distrib.*, vol. 10, no. 6, pp. 1401–1409, May 2016.